Electrochimica Acta 461 (2023) 142613

Contents lists available at ScienceDirect

Electrochimica Acta

journal homepage: www.journals.elsevier.com/electrochimica-acta

Design of NiNC single atom catalyst layers and AEM electrolyzers for stable and efficient CO_2-to-CO electrolysis: Correlating ionomer and cell performance

Jingyi Wang [a,1], Terrence R. Willson [b,1], Sven Brückner [a,1], Daniel K. Whelligan [b], Chunning Sun [c], Liang Liang [a], Xingli Wang [a], Peter Strasser [a,*], John Varcoe [b,*], Wen Ju [a,*]

[a] Department of Chemistry, Chemical Engineering Division, Technical University Berlin, Berlin 10623, Germany
[b] School of Chemistry and Chemical Engineering, University of Surrey, Guildford, Surrey, GU2 7XH, UK
[c] Inorganic Chemistry and Catalysis Group, Debye Institute for Nanomaterials Science, Utrecht University, Universiteitsweg 99, 3584 CG Utrecht, the Netherlands

A B S T R A C T

Deploying single-site NiNC catalysts in cathode catalyst layers of bipolar electrolyzer cells enables catalytic CO_2 valorization to e-CO at industrially relevant yields and efficiencies. The performance of the cathode layers is controlled by the turnover frequency of the active sites as well as mass transfer to and from the active sites. While the atomic scale structure-reactivity relations of single-site NiNC catalysts have been extensively studied, the mass transfer characteristics of single atom catalyst layers were poorly discussed. In this work, we design, build, and test NiNC catalyst layers using a novel set of distinct ion exchange ionomer materials and correlate the performance of cathode catalyst layers with their reactivity and stability in full single MEA electrolyzer cells. The Sustainion anion exchange ionomer delivered optimal performance, yielding about 90% CO faradaic efficiency up to 300 mA cm^{-2} and 15 h stable performance at 200 mA cm^{-2}. Our analysis attributes its favorable electrolyzer performance to its balanced conductivity and hydrophobicity, which mitigates electrode flooding while ensuring excellent ion and CO_2 transfer rates even at high current densities.

1. Introduction

Heavy dependence on fossil fuels and increasing human activities have contributed to climate change in recent decades. Global warming and ocean acidification threaten the living environment and natural resources for the current and next generations [1]. To mitigate this crisis, a number of different energy conversion and storage technologies based on renewable power are considered as future solutions. Critical components of future renewable energy technologies include green hydrogen production and its conversion into hydrogen fuel cells that have been set as a long-term strategy to decarbonize parts of the chemical and energy supply chains. For value chains related to carbon-/organic- chemicals, CO_2 capture, storage, and reuse technologies (Power-to-Carbon fuels) are considered essential [2–5].

In previous research, CO_2 conversion has been realized in different approaches, such as biochemical, thermochemical, photochemical, and electrochemical catalysis [6]. Among them, the CO_2 electrolysis is efficient and can directly convert CO_2 into value-add base chemicals such as CO and C_2H_4, [7,8] and more importantly, this conversion could be sustainably driven by the renewable electrisities [9,10].

CO_2 electrolysis performance largely relies upon the catalyst material and electrolyzer configurations. Kinetically, this reaction is sluggish and contains multiple electron-coupled proton transfer steps. Further, reacting in aqua conditions, the hydrogen evolution reaction (HER) competes strongly [11,12]. Hence, the catalyst selection for CO_2 electrolysis remains narrow, and most studies for high CO efficiency are on Au or Ag, the precious group metals (PGMs) [13]. For anion-exchange membrane (AEM) systems, Ag-derived gas diffusion electrodes (GDE) can exhibit industrial-interested activities ($>$ 200 mA cm^{-2} at reasonable cell voltages $<$ 3.5 V) [14–16]. However, the scarcity and cost of required PGM catalysts still limit their affordability for large-scale utilization. Hence, alternative catalytic candidates possessing comparable performance but built from abundant elements and via scalable synthetic routes are required.

Recently, a new class of non-PGM and nitrogen co-doped carbon-based (MNC) catalysts has drawn scientific attention for their specific structure and apparent catalytic reactivity [17–20]. This family catalyst contains unique coordinative single-metal active sites, structurally

* Corresponding authors.
E-mail addresses: pstrasser@tu-berlin.de (P. Strasser), j.varcoe@surrey.ac.uk (J. Varcoe), ju@tu-berlin.de (W. Ju).
[1] Authors contributed equally.

https://doi.org/10.1016/j.electacta.2023.142613
Received 30 January 2023; Received in revised form 24 April 2023; Accepted 17 May 2023
Available online 18 May 2023

suppressing the competition of unwanted HER [21,22]. Moreover, the porous carbon structure provides a larger active area over typical metal particles, offering a significant amount of active sites for reaction. As a result, the Ni-derived MNC (NiNC) model catalysts repeatedly outperformed the regular PGM candidates in mass-based activities [20, 23-26], offering a potential benchmark for large-scale CO_2 electrolysis.

The single-site NiNC catalysts have been extensively studied for atomic-level structure-activity relations at low current densities [27], while the mass transfer governing high current region was poorly discussed. Especially for transferring the model catalysts to flow electrolyzers, critical activity metrics of the resulting catalyst layer (CL) need to be considered. For instance, the apparent cell performance relies not only on the intrinsic turnover frequency of the active sites but also on the CO_2 reactant attainability (or the accessibility of the active sites) of the CLs. Meanwhile, the moisture on CLs must be carefully adjusted under reaction conditions since it serves the reaction and causes GDE flooding [28]. Moreover, the ion conductivity of the CL also plays an essential role in combination with the membrane at applied current densities [29–34]. All those factors could be manipulated by the optimal use of ionomer materials in CL preparation.

In this work, CLs were prepared with our standard baseline NiNC catalyst and six different ionomer materials, which act as conducting binders in the catalyst powder, forming mechanically stable CLs with tunable porosity, hydrophilicity, and ion conductivities [29–31]. The prepared GDEs were first screened for reaction kinetics in an H-type liquid cell to evaluate the synergistic effect between the catalyst and ionomers. Subsequently, they were assessed in an MEA-type electrolyzer for their apparent performance and stability in the mass transfer dominant region. We found that while the studied ionomers did not significantly affect reaction kinetics (< 30 mA cm^{-2}, in H-cell configuration), they did provide variable performances in the electrolyzer (> 200 mA cm^{-2}). This implies a significant influence of mass transfer on the catalytic interface. In our comparison, the Sustainion anion-exchange ionomer (< 15 wt% ionomer ratio with 1 mg cm^{-2} catalyst loading) delivers an optimal benchmark performance, yielding > 90% CO faradaic efficiency up to 300 mA cm^{-2} and with 15 h stable performance at 200 mA cm^{-2}, due to its optimized anion conductivity and hydrophobicity.

2. Results and discussion

We use our recently developed NiNC-IMI (Ni-imidazolate-derived) cathode catalyst for CO_2 electrolysis in an MEA-type electrolyzer. The catalyst synthesis, ink and GDE preparation, cell configuration, and testing platform are analogous to our earlier work [26], and those were represented in the **Supplementary Information (Supplementary Figures 1 to 4)**. All these offer a standard baseline to investigate the impact of ionomer materials on the NiNC-IMI-derived electrodes.

We selected six distinct ionomers for our comparisons, including a cation-exchange Nafion (Naf) counterpart and five anion exchange ionomers (AEIs): polystyrene-vinylbenzyl-methylimidazolium (Sus) [35], poly(aryl piperidinium) (PIP) [16,36], and three ETFE-based radiation-grafted AEIs with benzyl-*N*-methylpyrrolidinium (MPY), benzyltrimethylammonium (TMA), and *N*-methylpiperidinium (MPIP) cationic headgroups [37]. Their functional ion-exchange headgroups, backbone structures, and other parameters are given in Fig. 1 and **Supplementary Table 1**. Our prepared MPY, TMA, and MPIP possess IEC (ion exchange capacity) values around 2.00 mmol g^{-1}, double the commercial Sus ionomer. Meanwhile, an ionomer-free catalyst ink/layer was given as a reference.

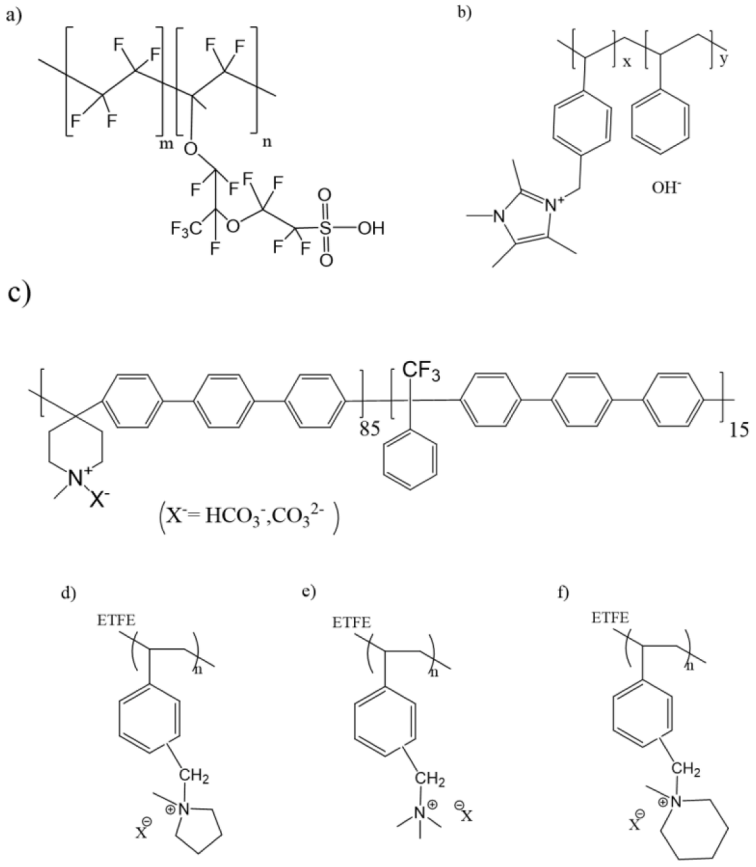

Fig. 1. The chemical structures of a) the Nafion cation-exchange ionomer and (b-f) the anion-exchange ionomers (AEI) used in this study: b) Sustainion (IEC: 0.95 mmol g^{-1}), c) PiperION (IEC: 2.4 mmol g^{-1}) and ETFE-based radiation-grafted AEI powders with d) MPY (IEC: 2.0 ± 0.02 mmol g^{-1}), e) TMA (IEC: 2.09 ± 0.01 mmol g^{-1}), and f) MPIP (IEC: 1.85 ± 0.05 mmol g^{-1}) head-groups.

Considering the ionomers have different intrinsic chemical structures (added crosslinking in Sus, main-chain cations for PIP, polycationic grafts for MPY, TMA, and MPIP), these could lead to differing structures, porosity, and morphologies when bound to catalyst powders [38]. For this, Dynamic Light Scattering (DLS) was conducted to characterize the catalyst ink. In Fig. 2, the left axis shows the catalyst powder's average hydrodynamic radius accompanied by different ionomers. We found that all ionomers can maintain a constant radius of around 300 nm within 10 min (comparable to the spray-coating time), but the MPY, TMA, and MPIP lead to agglomeration when extended to 40 min. Next, ink transparency (right axis) represents the catalyst ink suspension's average powder concentration and stability. All inks show no phase separation within 40 mins.

The catalyst ink was later sprayed on our gas diffusion electrode (DN908) to a catalyst loading of 1 mg cm^{-2}. The top view of the catalyst layer was measured using Scanning Electron Microscope (SEM), and the images are presented in **Supplementary Figure 5 - 9**, showing homogeneously distributed channels for gas diffusion/convection. Furthermore, contact angle measurements were performed on those catalyst layers (Fig. 2), and only the Naf and Sus turned out to be hydrophobic. In brief, the ionomers in our control measurements merely impact their hydrophobicity in our characteristic methodologies.

All those sprayed CLs with 1 mg cm^{-2} NiNC-IMI catalyst loading and 15 wt% ionomers (~ 0.176 mg cm^{-2}) were tested in our liquid H-cell configuration. In addition, cyclic voltammetry was first performed in CO_2-saturated 0.5 M $KHCO_3$ between 0.0 and 0.6 V_{RHE} with different scan rates (**Supplementary Figure 10 - 11**) to compare their electrochemical surface area (ECSA). As a result, the Naf and Sus have only half double layer current (the ECSA) compared to other counterparts, which is suspected due to their hydrophobicity.

The electrochemical performance of our catalyst with different ionomers was screened in the potential region from −0.4 to −0.85 V_{RHE} (Fig. 3). Overall, the catalytic CO activity was barely influenced by the ionomer materials, showing consistent CO onset and similar Tafel-Slop (Fig. 3c). The CO formation onsets near −0.5 V_{RHE} and reaches the peak faradaic efficiency (FE_{CO} ~ 80%) at −0.7 V_{RHE}. The HER activity is slightly improved by the MPY while suppressed by Sus. With all those ionomers, the FE_{CO} activity meets a plateau at around 15 mA cm^{-2} total current density (Fig. 3f). In brief, the ionomer materials and ratio (up to 50 wt%, see **Supplementary Figure 2f** and **Supplementary Figure 12**) only slightly decrease the geometric activity, possibly due to a capping effect.

Next, we assess those ionomers in the MEA-type electrolyzer for their effects on mass transfer at high current densities (Fig. 4). The assembling protocol is written in the **Supplementary Information**, using our synthesized radiation-grafted ETFE-based MPIP anion exchange membrane (RG-E-MPIP-AEM, IEC = 1.78 ± 0.04 mmol g^{-1}, hydrated thickness: ~61 μm. Detail is given in **Supplementary Information**) [37,39]. The catalytic performance tests were performed from −50 mA cm^{-2} to −500 mA cm^{-2} at 45 °C, with the ionomer loading of 15 wt%. Each current step was kept stationary for 15 min for product quantification. Consistent with the H-cell screening, only H_2 and CO are found as the major products, and their faradaic efficiency sums above 90% (see Fig. 4a, b). However, unlike the trends observed in H-cell, our studied ionomers perform differently in the MEA electrolyzer. For example, the Naf shows only 50% FE_{CO} in the MEA configuration while requiring higher cell potentials (~ 3.5 V for 50 mA cm^{-2}, Fig. 4c). This could be attributed to the incompatibility between the cation exchange headgroups and the anion exchange groups in our RG-E-MPIP-AEM (at 45 °C), limiting the through-plane mass transfer during the reaction.

By contrast, for all AEIs, CO is the dominant product up to 200 mA cm^{-2}, and a distinction appears when approaching higher current densities. Only the Sus and TMA provide over 90% FE_{CO} at 300 mA cm^{-2}, whereas the others show a sharp drop. The polarization curves of all those AEIs (Fig. 4c) fall in a similar domain. Nonetheless, compared with the CL without ionomer, the presence of the ionomer causes the potential penalty, also reflected in our galvanic electrochemical impendence spectroscopy (GEIS, **Supplementary Figure 13**) and Sus ionomer ratio study (**Supplementary Figure 14**).

Last, we investigate the performance stability of the CLs with different ionomers at 200 mA cm^{-2} current density. FE_{CO} of the non-ionomer reference CL constantly keeps above 95% for 10 h and displays gradual degradation after that (along with raising cell voltage, Fig. 5a). Remarkably, in this comparison, the Sus ionomer could improve the stability to 15 h, although its performance drastically collapses afterward. On the contrary, other AEIs only shorten the stability to about 5 h. Briefly summarizing, only the Sus and TMA ionomers positively contribute to the catalytic reactivity, while only the Sus could extend the stability.

3. Conclusion

We deployed six ionomer materials for our NiNC-IMI catalyst for CO_2 electrolysis and comprehensively studied their impacts on catalyst layer preparation and catalytic performance. In our characterization, only minor differences were found in catalyst ink states (average powder size and suspension state) within a short period (< 10 min, according to our spray coating procedure). The catalyst layer morphology from the top view also shows only slight variations. The electrochemical active surface area (ECSA) depends on the ionomer candidates. For instance, Naf and Sus offer only half of the double layer capacity (equivalent to ECSA) with the presence of other candidates, which we suspect is due to the

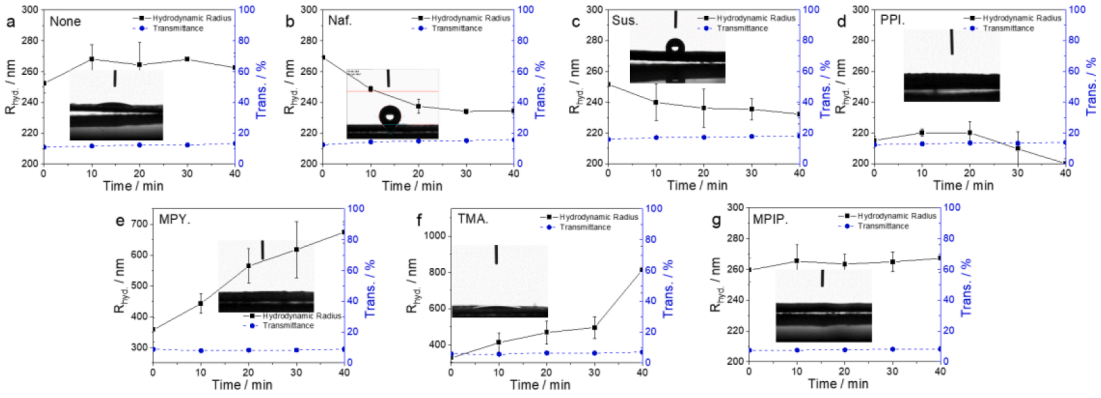

Fig. 2. Hydrodynamic Radius and Transmittance of the dilute catalyst ink with different ionomers based on the time. Pictures of the contact angle of the gas diffusion electrode with different ionomers: a) without ionomer, b) Naf, c) Sus, d) PPI, e) MPY, f) TMA, and g) MPIP. Dynamic light scattering (DLS) and transmittance tests were carried out using an Anton Paar Litesizer 500 equipped with a 658 nm laser at 8.5 mm height. Time-lapse size evolution (hydrodynamic radius) was obtained at a backscattering angle of 175° All data were collected by measuring the sample solution in a 10 mm path length cuvette with a filling height of 10 mm.

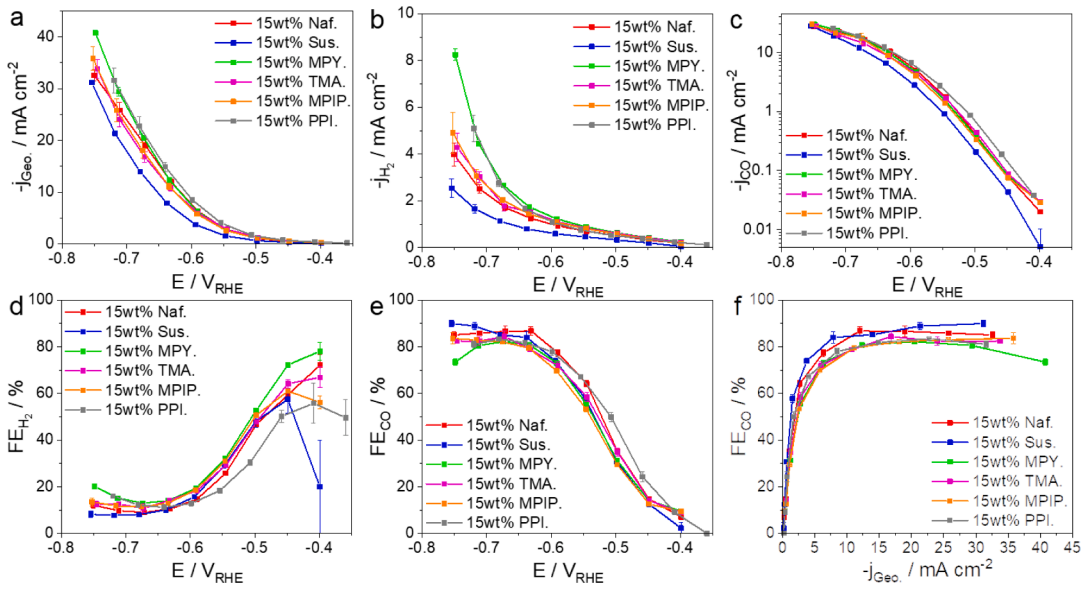

Fig. 3. The catalytic performance of NiNC-IMI-based electrodes with different ionomers assessed in liquid phase H-cell at low cathodic potentials and current densities. a) Geometric current density ($-j_{Geo.}$), b) H_2 partial current density ($-j_{H2}$), c) CO partial current density ($-j_{CO}$) in logarithm, d) Faradaic efficiency of H_2 (FE_{H2}), e) faradaic efficiency of CO (FE_{CO}), as a function of iR-correct cathodic potential, and f) faradaic efficiency of CO as a function of geometric current density. Reaction condition: 0.5 M $KHCO_3$ purged by 30 mL min^{-1} CO_2 at room temperature; catalyst loading: 1 mg cm^{-2} on 1 cm^2 electrode area.

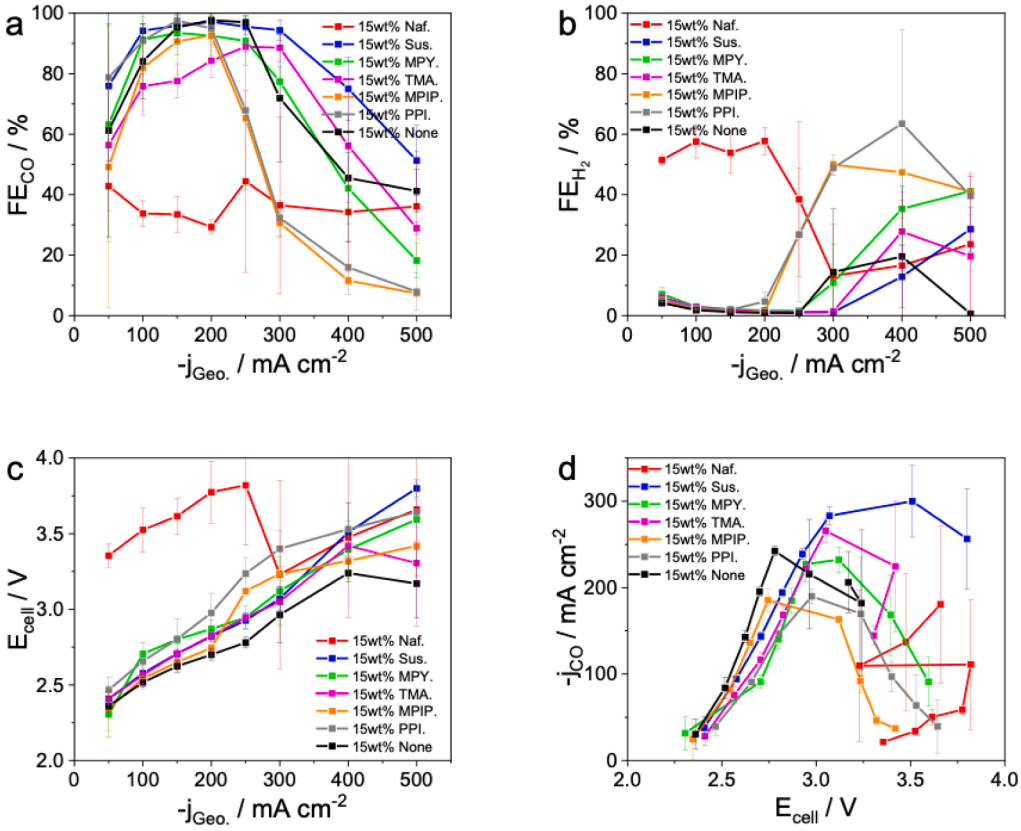

Fig. 4. The catalytic performance of NiNC-IMI-based GDEs with different ionomers in MEA-electrolyzer. a) Faradaic efficiency of CO (FE_{CO}), b) faradaic efficiency of H_2 (FE_{H2}), c) required cell potential (without iR-correction) as a function of applied current density, and d) CO partial current density as a function of cell potential. Reaction condition: anolyte flow: 20 mL min^{-1} 0.1 M $KHCO_3$; cathode gas flow: 60 mL min^{-1} humidified CO_2; both chambers are separated by our RG-E-MPIP-AEM, IEC: 1.78 ± 0.04 mmol g^{-1}; [37] reaction temperature: 45 °C; catalyst loading: 1 mg cm^{-2} on 5 cm^2 electrode area.

hydrophobicity. Hence, in the later H-cell performance screening (the low current region in the liquid phase), the CO activity as a function of the potential of all candidates resembles, indicating similarities in intrinsic reaction kinetics and exposure of the active sites.

The ionomer headgroups play a significant role in the MEA-electrolyzer. The Naf exhibits above 50% faradaic efficiency to unwanted HER and demands a larger potential for certain currents. We assume the Naf, with cation exchange headgroups, could glue to the AEM headgroups or form a bipolar junction at the CL interface, blocking the through-plane transfer during the reaction. This has been demonstrated in part in our galvanic impedance spectroscopy.

By contrast, all AEIs deliver better synergy with the RT-E-MPIP-AEM. We observe over 80% FE_{CO} up to 200 mA cm^{-2} with less potential demand, consistent with the GEIS profiles in the low-frequency region

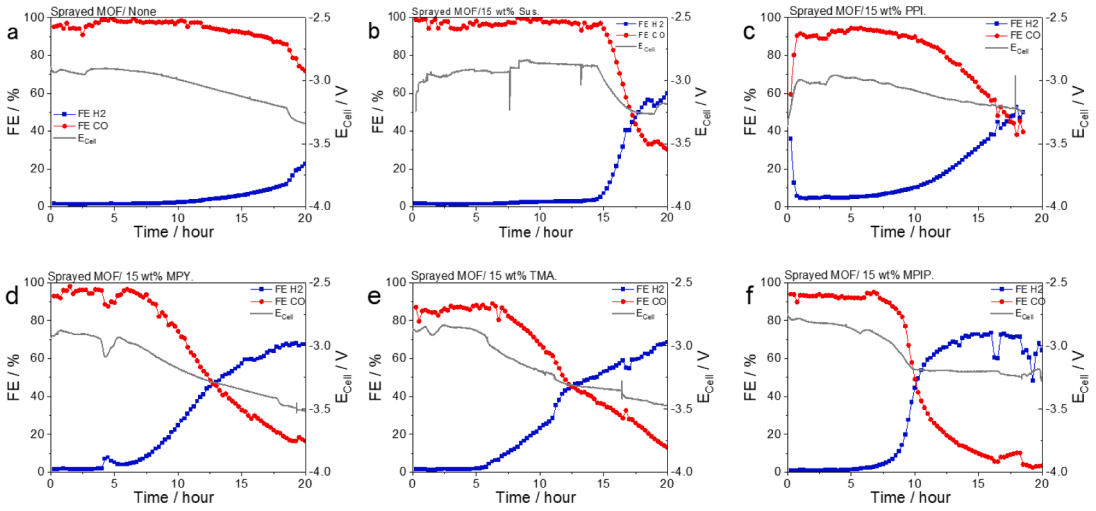

Fig. 5. The stability test of NiNC-IMI-based GDEs with different ionomers in MEA-electrolyzer. Faradaic efficiency of CO (FE_{CO}, red, left axis), faradaic efficiency of H_2 (FE_{H2}, blue, left axis), and cell voltage (gray, right axis) at 200 mA cm^{-2} current density as a function of time. NiNC-IMI-GDE a) without ionomer, with b) Naf, c) Sus, d) PPI, e) MPY, f) TMA, and g) MPIP. Reaction condition: anolyte flow: 20 mL min^{-1} 0.1 M $KHCO_3$; cathode gas flow: 60 mL min^{-1} humidified CO_2; both chambers are separated by the MPIP RG-AEM; reaction temperature: 45 °C; catalyst loading: 1 mg cm^{-2} on 5 cm^2 electrode area.

(mass transfer related). However, at higher current densities, the selectivity and stability can hardly be correlated with the IEC values. For instance, the Sus (with IEC of 0.9 mmol g^{-1}) delivers promising FE_{CO} at 300 mA cm^{-2}. On the other hand, our produced TMA (~2.0 mmol g^{-1}), MPY (~2.00 mmol g^{-1}), MPIP (~1.85 mmol g^{-1}), and the commercial PPI (~2.4 mmol g^{-1}) with high IEC values bring only benefits to mass transfer (accordingly to the cell potential) but cause "easy flooding" during the reaction, blocking the CO_2 transfer in the CL. Therefore, we deduce that hydrophobicity is more necessary than the IEC of the ionomers for the NiNC-IMI powder catalyst.

To the ionomer ratio in the catalyst layer, we down-select the Sus ionomer and vary the ratio from 8 wt% to 50 wt%. As presented in **Supplementary Figure 14**, high (> 15 wt%) Sus AEI loadings cause potential penalties and mitigate the selectivity towards CO. On the contrary, low loadings (8 wt% and 15 wt%) could maintain the FE_{CO} at high current densities (250 to 500 mA cm^{-2}). Therefore, we suspect high loading forms an additional inactive layer, limiting the anions' attainability between the catalyst and membrane.

Overall, in this ionomer study, the Sus AEI, with a reasonable ratio (below 15 wt%), improves the catalytic reactivity and performance stability of the NiNC-IMI-GDE, delivering 90% FE_{CO} at 300 mA cm^{-2} and 15 h of performance stability at 200 mA cm^{-2}. These should thank its moderate and balanced anion conductivity and hydrophobicity, which prevents the CL/GDE flooding while conducting high current density CO_2 electrolysis [28]. Beyond the scope of this work, chemical and mechanical stability of the membrane and ionomer materials is also highly recommended. Those can maintain the IEC, water uptake, hydrophobicity/hydrophilicity the essential metrics of catalytic interface for high current and long-term CO_2 electrolysis [40,41].

Data availability statement

The data that support the findings of this study are available from the corresponding author upon reasonable request.

Credit author statement

J. Varcoe, P. Strasser, and W. Ju designed and supervised the study. J. Wang and S. Brückner performed the electrochemical assessments. T. Willson synthesized the membrane and ionomer materials. Other co-authors provided support for some of the characteristic analyses. All authors contributed to the interpretation of the results and the writing of the manuscript.

Declaration of Competing Interest

The authors declare that they have no known competing financial interests or personal relationships that could have appeared to influence the work reported in this paper.

Acknowledgments

The research leading to these results has received funding from the European Union's Horizon 2020 research and innovation program under grant agreement no. 851441, SELECTCO2, the European Union's Horizon 2020 research and innovation program under grant agreement no. 101006701, ECOFUEL, the Deutsche Forschungsgemeinschaft (DFG, German Research Foundation, grant No. STR 596/18–1 and LI 4184/2–1), and the Initiative and Networking Fund of the Helmholtz Association (grant agreement No.KA2-HSC-12, 'A Comprehensive Approach to Harnessing the Innovation Potential of Direct Air Capture and Storage for Reaching CO2-Neutrality', DACStorE). We also thank Prof. Michael Gradzielski for the equipment and discussion on DLS analysis.

Supplementary materials

Supplementary material associated with this article can be found, in the online version, at doi:10.1016/j.electacta.2023.142613.

References

[1] J.M. Pandolfi, S.R. Connolly, D.J. Marshall, A.L. Cohen, Projecting coral reef futures under global warming and ocean acidification, Science 333 (6041) (2011) 418–422.
[2] D. D.W. Keith, G. Holmes, St. Angelo, K. Heidel, A process for capturing CO2 from the atmosphere Joule 2 (8) (2018) 1573–1594.
[3] K. Michael, A. Golab, V. Shulakova, J. Ennis-King, G. Allinson, S. Sharma, T. Aiken, Geological storage of CO2 in saline aquifers—a review of the experience from existing storage operations, Int. J. Greenhouse Gas Control 4 (4) (2010) 659–667.
[4] Y. Teng, D. Zhang, Long-term viability of carbon sequestration in deep-sea sediments, Sci. Adv. 4 (7) (2018) eaao6588.
[5] S. Fawzy, A.I. Osman, J. Doran, D.W. Rooney, Strategies for mitigation of climate change: a review, Environ. Chem. Lett. 18 (6) (2020) 2069–2094.
[6] C. Chen, J.F. Khosrowabadi Kotyk, S.W. Sheehan, Progress toward commercial application of electrochemical carbon dioxide reduction, Chem 4 (11) (2018) 2571–2586.
[7] J.E. Huang, F. Li, A. Ozden, A. Sedighian Rasouli, F.P. García de Arquer, S. Liu, S. Zhang, M. Luo, X. Wang, Y. Lum, Y. Xu, K. Bertens, R.K. Miao, C.-T. Dinh,

D. Sinton, E.H. Sargent, CO2 electrolysis to multicarbon products in strong acid, Science 372 (6546) (2021) 1074–1078.
[8] X. Nie, W. Luo, M.J. Janik, A. Asthagiri, Reaction mechanisms of CO2 electrochemical reduction on Cu(111) determined with density functional theory, J. Catal. 312 (2014) 108–122.
[9] F.J. Qi Lu, Electrochemical CO2 reduction: electrocatalyst, reaction mechanism, and process engineering, Nano Energy 29 (2016) 439–456.
[10] S. Chu, Y. Cui, N. Liu, The path towards sustainable energy, Nat. Mater. 16 (1) (2016) 16–22.
[11] Y. Hori, Electrochemical CO2 Reduction on Metal Electrodes, in: C.G. Vayenas, R. E. White, M.E. Gamboa-Aldeco (Eds.), Modern Aspects of Electrochemistry, Springer New York, New York, NY, 2008, pp. 89–189. Eds.
[12] W. Ju, A. Bagger, N. Leonard, X. Wang, J. Rossmeisl, P. Strasser, Chapter 4 nanostructures for CO2 reduction: from theoretical insight to material design. Carbon Dioxide Electrochemistry: Homogeneous and Heterogeneous Catalysis, The Royal Society of Chemistry, 2021, pp. 151–196.
[13] A. Ozden, Y. Liu, C.-T. Dinh, J. Li, P. Ou, F.P. García de Arquer, E.H. Sargent, D. Sinton, Gold adparticles on silver combine low overpotential and high selectivity in electrochemical CO2 conversion, ACS Appl. Energy Mater. 4 (8) (2021) 7504–7512.
[14] T. Zheng, K. Jiang, H. Wang, Recent advances in electrochemical CO2 -to-CO conversion on heterogeneous catalysts, Adv. Mater. 30 (48) (2018), e1802066.
[15] D.L.T. Nguyen, Y. Kim, Y.J. Hwang, D.H. Won, Progress in development of electrocatalyst for CO2 conversion to selective CO production, Carbon Energy 2 (1) (2019) 72–98.
[16] B. Endrődi, E. Kecsenovity, A. Samu, T. Halmágyi, S. Rojas-Carbonell, L. Wang, Y. Yan, C. Janáky, High carbonate ion conductance of a robust PiperION membrane allows industrial current density and conversion in a zero-gap carbon dioxide electrolyzer cell, Energy Environ. Sci. 13 (11) (2020) 4098–4105.
[17] D.-H. Nam, O. Shekhah, G. Lee, A. Mallick, H. Jiang, F. Li, B. Chen, J. Wicks, M. Eddaoudi, E.H. Sargent, Intermediate binding control using metal–organic frameworks enhances electrochemical CO2 reduction, J. Am. Chem. Soc. 142 (51) (2020) 21513–21521.
[18] H. Wan, Y. Jiao, A. Bagger, J. Rossmeisl, Three-dimensional carbon electrocatalysts for CO2 or CO reduction, ACS Catal. 11 (2) (2021) 533–541.
[19] C. Kim, T. Eom, M.S. Jee, H. Jung, H. Kim, B.K. Min, Y.J. Hwang, Insight into electrochemical CO2 reduction on surface-molecule-mediated Ag nanoparticles, ACS Catal. 7 (1) (2017) 779–785.
[20] W. Ju, A. Bagger, G.-.P. Hao, A.S. Varela, I. Sinev, V. Bon, B. Roldan Cuenya, S. Kaskel, J. Rossmeisl, P. Strasser, Understanding activity and selectivity of metal-nitrogen-doped carbon catalysts for electrochemical reduction of CO2, Nat. Commun. 8 (1) (2017) 944.
[21] A. Bagger, W. Ju, S. Varela Ana, P. Strasser, J. Rossmeisl, Electrochemical CO2 reduction: a classification problem, ChemPhysChem 18 (22) (2017) 3266–3273.
[22] A. Bagger, W. Ju, A.S. Varela, P. Strasser, J. Rossmeisl, Single site porphyrine-like structures advantages over metals for selective electrochemical CO2 reduction, Catal. Today 288 (2017) 74–78.
[23] A.S. Varela, W. Ju, A. Bagger, P. Franco, J. Rossmeisl, P. Strasser, Electrochemical reduction of CO2 on metal-nitrogen-doped carbon catalysts, ACS Catal. 9 (8) (2019) 7270–7284.
[24] T. Möller, W. Ju, A. Bagger, X. Wang, F. Luo, T. Ngo Thanh, A.S. Varela, J. Rossmeisl, P. Strasser, Efficient CO2 to CO electrolysis on solid Ni–N–C catalysts at industrial current densities, Energy Environ. Sci. 12 (2) (2019) 640–647.
[25] C. Li, W. Ju, S. Vijay, J. Timoshenko, K. Mou, D.A. Cullen, J. Yang, X. Wang, P. Pachfule, S. Brückner, H.S. Jeon, F.T. Haase, S.-.C. Tsang, C. Rettenmaier, K. Chan, B.R. Cuenya, A. Thomas, P. Strasser, Covalent Organic Framework (COF) Derived Ni-N-C Catalysts for Electrochemical CO2 Reduction: unraveling fundamental kinetic and structural parameters of the active sites, Angewandte Chemie International Edition 61 (15) (2022), e202114707.
[26] F. Q. S. Brückner, W. Ju, D. Galliani, A. Testolin, M. Klingenhof, et al., Design and Diagnosis of high-performance CO2-to-CO electrolyzer cells ChemRxiv (2023). *Cambridge: Cambridge Open Engage*
[27] S. Liang, L. Huang, Y. Gao, Q. Wang, B. Liu, Electrochemical reduction of CO2 to CO over Transition Metal/N-doped carbon catalysts: the Active Sites and Reaction Mechanism, Adv. Sci. 8 (24) (2021), 2102886.
[28] K. Yang, R. Kas, W.A. Smith, T. Burdyny, Role of the carbon-based gas diffusion layer on flooding in a gas diffusion electrode cell for electrochemical CO2 reduction, ACS Energy Lett. 6 (1) (2021) 33–40.
[29] M. So, K. Park, Y. Tsuge, G. Inoue, A particle based ionomer attachment model for a fuel cell catalyst layer, J. Electrochem. Soc. 167 (1) (2020), 013544.
[30] S. Ott, A. Orfanidi, H. Schmies, B. Anke, H.N. Nong, J. Hubner, U. Gernert, M. Gliech, M. Lerch, P. Strasser, Ionomer distribution control in porous carbon-supported catalyst layers for high-power and low Pt-loaded proton exchange membrane fuel cells, Nat. Mater. 19 (1) (2020) 77–85.
[31] R. Alink, R. Singh, P. Schneider, K. Christmann, J. Schall, R. Keding, N. Zamel, Full parametric study of the influence of ionomer content, catalyst loading and catalyst type on oxygen and ion transport in PEM fuel cell catalyst layers, Molecules 25 (7) (2020) 1523.
[32] M. Ma, E.L. Clark, K.T. Therkildsen, S. Dalsgaard, I. Chorkendorff, B. Seger, Insights into the carbon balance for CO2 electroreduction on Cu using gas diffusion electrode reactor designs, Energy Environ. Sci. 13 (3) (2020) 977–985.
[33] M. Ma, S. Kim, I. Chorkendorff, B. Seger, Role of ion-selective membranes in the carbon balance for CO2 electroreduction via gas diffusion electrode reactor designs, Chem. Sci. 11 (33) (2020) 8854–8861.
[34] S. Garg, C.A. Giron Rodriguez, T.E. Rufford, J.R. Varcoe, B. Seger, How membrane characteristics influence the performance of CO2 and CO electrolysis, Energy Environ. Sci. 15 (11) (2022) 4440–4469.
[35] Z. Liu, H. Yang, R. Kutz, R.I. Masel, CO2 Electrolysis to CO and O2 at high selectivity, stability and efficiency using sustainion membranes, J. Electrochem. Soc. 165 (15) (2018) J3371.
[36] J. Wang, Y. Zhao, B.P. Setzler, S. Rojas-Carbonell, C. Ben Yehuda, A. Amel, M. Page, L. Wang, K. Hu, L. Shi, S. Gottesfeld, B. Xu, Y. Yan, Poly(aryl piperidinium) membranes and ionomers for hydroxide exchange membrane fuel cells, Nat. Energy 4 (5) (2019) 392–398.
[37] C.A. Giron Rodriguez, B.Ó. Joensen, A.B. Moss, G.O. Larrazábal, D.K. Whelligan, B. Seger, J.R. Varcoe, T.R. Willson, Influence of headgroups in ethylene-tetrafluoroethylene-based radiation-grafted anion exchange membranes for CO2 electrolysis, ACS Sustain. Chem. Eng. (2023).
[38] C. Lantman, W. MacKnight, R. Lundberg, Structural properties of ionomers, Ann. Rev. Mater. Sci. 19 (1) (1989) 295–317.
[39] A.L. Gonçalves Biancolli, D. Herranz, L. Wang, G. Stehlíková, R. Bance-Soualhi, J. Ponce-González, P. Ocón, E.A. Ticianelli, D.K. Whelligan, J.R. Varcoe, E. I. Santiago, ETFE-based anion-exchange membrane ionomer powders for alkaline membrane fuel cells: a first performance comparison of head-group chemistry, J. Mater. Chem. A 6 (47) (2018) 24330–24341.
[40] A. Zhegur, N. Gjineci, S. Willdorf-Cohen, A.N. Mondal, C.E. Diesendruck, N. Gavish, D.R. Dekel, Changes of anion exchange membrane properties during chemical degradation, ACS Appl. Polym. Mater. 2 (2) (2020) 360–367.
[41] B. Hasa, L. Cherniack, R. Xia, D. Tian, B.H. Ko, S. Overa, P. Dimitrakellis, C. Bae, F. Jiao, Benchmarking anion-exchange membranes for electrocatalytic carbon monoxide reduction, Chem. Catal. 3 (1) (2023), 100450.